A Supervised Learning Framework for Automatic Prostate Segmentation in Trans Rectal Ultrasound Images

Soumya Ghose[1,2], Jhimli Mitra[1,2], Arnau Oliver[1], Robert Martí[1],
Xavier Lladó[1], Jordi Freixenet[1], Joan C. Vilanova[3], Josep Comet[4],
Désiré Sidibé[2], and Fabrice Meriaudeau[2]

[1] Computer Vision and Robotics Group, University of Girona, Campus Montilivi,
Edifici P-IV, Av. Lluís Santaló , s/n, 17071 Girona, Spain
[2] Laboratoire Le2I - UMR CNRS 5158, Université de Bourgogne,
12 Rue de la Fonderie, 71200 Le Creusot, France
[3] Girona Magnetic Resonance Imaging Center, Girona, Spain
[4] University Hospital Dr. Josep Trueta, Girona, Spain

Abstract. Heterogeneous intensity distribution inside the prostate gland, significant variations in prostate shape, size, inter dataset contrast variations, and imaging artifacts like shadow regions and speckle in Trans Rectal Ultrasound (TRUS) images challenge computer aided automatic or semi-automatic segmentation of the prostate. In this paper, we propose a supervised learning schema based on random forest for automatic initialization and propagation of statistical shape and appearance model. Parametric representation of the statistical model of shape and appearance is derived from principal component analysis (PCA) of the probability distribution inside the prostate and PCA of the contour landmarks obtained from the training images. Unlike traditional statistical models of shape and intensity priors, the appearance model in this paper is derived from the posterior probabilities obtained from random forest classification. This probabilistic information is then used for the initialization and propagation of the statistical model. The proposed method achieves mean Dice Similarity Coefficient (DSC) value of 0.96±0.01, with a mean segmentation time of 0.67±0.02 seconds when validated with 24 images from 6 datasets with considerable shape, size, and intensity variations, in a leave-one-patient-out validation framework. The model achieves statistically significant t-test p-value<0.0001 in mean DSC and mean mean absolute distance (MAD) values compared to traditional statistical models of shape and intensity priors.

Keywords: Prostate Segmentation, Random Forest, Statistical Shape and Posterior Probability Models, Ultrasound.

1 Introduction

Prostate cancer is the most commonly diagnosed cancer in North America and accounted for 33,000 estimated deaths in 2011 [1]. Accurate prostate

segmentation in TRUS may aid in radiation therapy planning, motion monitoring, biopsy needle placement and multimodal image fusion between TRUS and magnetic resonance imaging (MRI) to improve malignant tissue extraction during biopsy [19]. However, accurate computer aided prostate segmentation from TRUS images is a challenging task due to low contrast of TRUS images, speckle, and shadow artifacts. Moreover, inter-patient prostate shape, size and deformation may vary significantly and heterogeneous intensity distribution inside the prostate gland may introduce further challenges in automatic prostate segmentation.

Deformable models and statistical shape models are commonly used for prostate segmentation in TRUS images. For example Badiei et al. [2] used a deformable model of warping ellipse and Ladak et al. [14] used discrete dynamic contour to achieve semi-automatic prostate segmentation. However, prostate segmentation during TRUS guided biopsy procedures should necessarily be automatic. Shen et al. [18] and Zhan et al. [20] presented an automatic method that incorporated a priori shape and texture information from Gabor filters to produce accurate prostate segmentation. However, the method is computationally expensive and probably unsuitable for TRUS guided prostate intervention [19]. In recent years, Cosio et al. [6] reported an automatic method for prostate segmentation with active shape models [4]. However, the computationally intensive optimization framework of genetic algorithm is unsuitable for TRUS guided intervention.

In recent years, supervised machine learning methods have been adopted for solving prostate segmentation problems in medical images [15,10]. Motivated by these approaches we propose a novel prostate segmentation method in which appearance and spatial context based information from the training images are used to classify a new test image to achieve probabilistic classification of the prostate. Further, statistical shape and appearance model derived from PCA of prostate shape and posterior probabilistic values of the prostate region of the training TRUS images are propagated in a multi-resolution framework to segment a test image. The key contributions of this work are:

– The use of random forest classification framework to obtain a soft classification of the prostate.
– Using such information in training, automatic initialization and propagation of our model.

The performance of our method is compared with the traditional active appearance model (AAM) [5] and also with our previous work [11]. Compared to the use of intensity as in [5] and to the use of texture obtained from quadrature filter in [11], the posterior probabilistic information is used to train, initialize and propagate our model. Statistically significant improvement is achieved when validated with 24 images that have significant shape, size, and contrast variations of the prostate in a leave-one-patient-out validation framework.
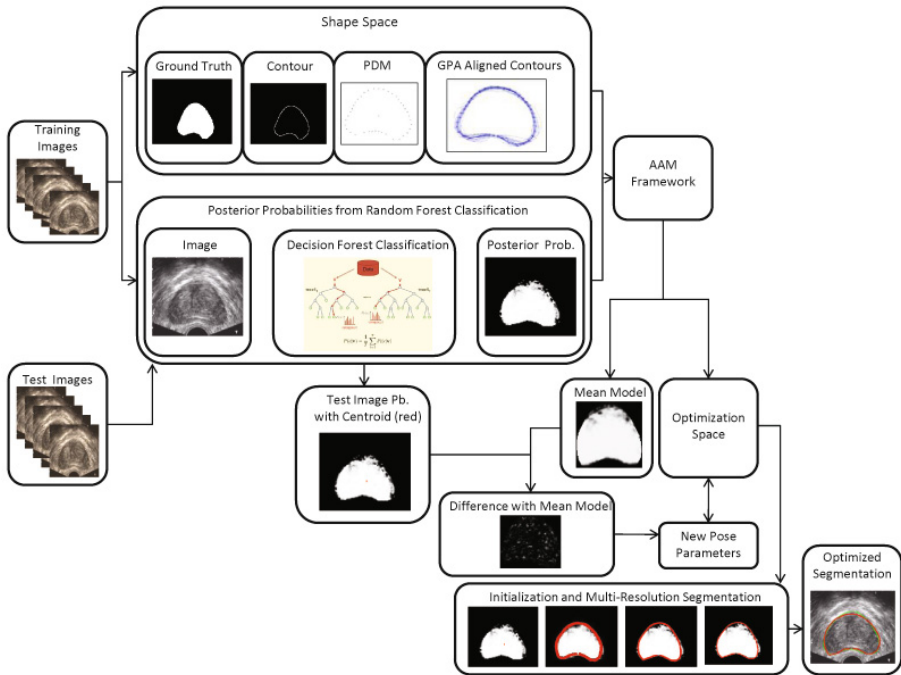
Fig. 1. Schematic representation of our approach. Abbreviations used PDM = Point Distribution Model, GPA = Generalized Procustes Analysis, Pb. = Probability.

2   Proposed Segmentation Framework

The proposed method is developed on two major components: 1) Supervised learning framework of decision trees (random forest) to determine the posterior probability of a pixel being prostate, and 2) adapting statistical models of shape and intensity priors to incorporate the posterior probabilities of the prostate region for training, initialization and propagation of the parametric model. We present the random forest framework for determining posterior probability of the prostate region, followed by our statistical shape and probability prior model of the prostate region in the following subsections. The schema of our proposed method is illustrated in Fig. 1.

2.1   Random Forest Based Probabilistic Classification

In traditional AAM [5], the point distribution model (PDM) [4] of the contour is aligned to a common reference frame by generalized Procrustes analysis [13]. Intensities are warped into correspondence using a piece-wise affine warp and sampled from a shape-free reference. Intensity distribution inside the prostate region may vary significantly from one dataset to another depending on the ultrasound image acquisition parameters and nature of the prostate tissue of a

patient. Hence, the use of intensity distribution of the prostate region to build the texture model as in traditional AAM introduces larger variations producing an inaccurate texture model that adversely affects segmentation results. To reduce the inter-dataset intensity variations and intensity variations inside the prostate region, we propose to determine the posterior probability of the image pixels being prostate in a supervised learning framework and use PCA of the posterior probabilities of the prostate region to build our appearance model.

Our approach of using pixel location to determine the prior position information of the prostate is based on the works of Cosio et al. [6] and Shen et al. [18]. Both used prior prostate location information in TRUS images to automatically initialize their model. Cosio et al. [6] used a 3D feature vector of pixel location and intensity value to classify and localize prostate in TRUS images for initialization of their model. Similarly, Shen et al. [18] proposed to use the relative position of the prostate with respect to the TRUS probe (located at the center of the base line of the TRUS image) for initialization. More recently Li et al. [15] used a spatial context based machine learning approach to achieve a probabilistic segmentation of the prostate. Motivated by these approaches we propose a supervised learning framework that exploits the location and image feature information of the prostate in TRUS images to determine the posterior probability of the prostate region.

In this paper, the probabilistic classification addressed by supervised random decision forest may be formalized as a soft classification of pixels into either background or prostate. Decision trees are discriminative classifiers which are known to suffer from over-fitting. However, a random decision forest achieves better generalization by growing an ensemble of many independent decision trees on a random subset of the training data and by randomizing the features made available at each node during training [10].

During **training**, to minimize the pose and intensity variations, our datasets are rigidly aligned based on intensities. We have used Evangelidis et al. [9] for rigid alignment. The inter-patient intensity variations are linearly normalized between 0 and 1. The data consists of a collection of features obtained from 3×3 neighborhood of pixels, each centered at $V = (X, F)$. Where, $X = (x, y)$ denotes the position of the pixel associated with a feature vector F. The mean and standard deviation of the 3×3 pixel neighborhood are used as the feature vector F. Each tree $\tau_i, i = 1, \ldots, T$ in the decision forest receives the full set V, along with the label and the root node and selects a test to split V into two subsets to maximize information gain. A test consists of a feature (like the mean of a pixel neighborhood) and a feature response threshold. The left and the right child nodes receive their respective subsets of V and the process is repeated at each child node to grow the next level of the tree. Growth is terminated when either information gain is minimum or the tree has grown to maximum depth. Each decision tree in the forest is unique as each tree node selects a random subset of features and threshold.

During **testing**, the test image is rigidly aligned to the same frame of the training datasets and its intensities are normalized. The pixels are routed to one
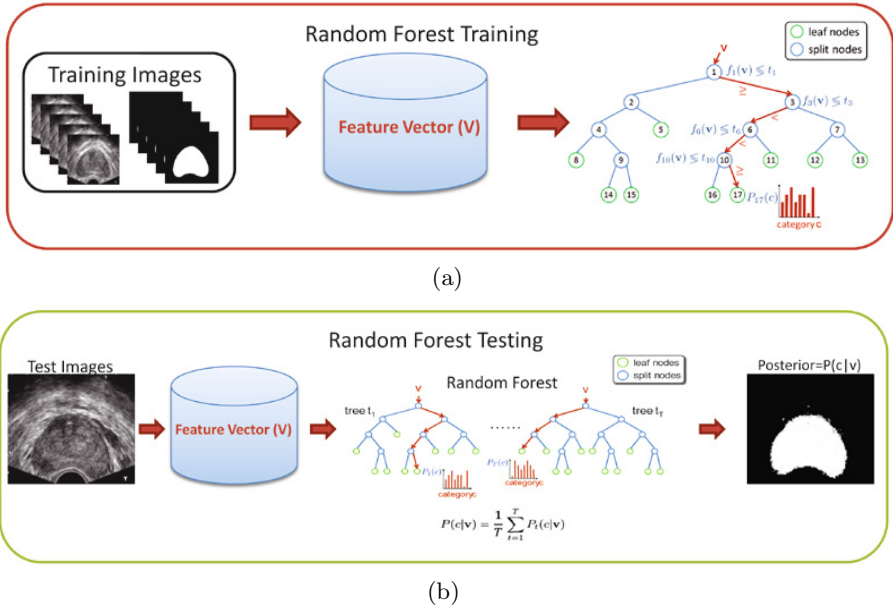
(a)

(b)

Fig. 2. Random forest classification framework (a) Random forest training (b) Random forest classification with a test image

leaf in each tree by applying the test (selected during training). Each pixel of the test dataset is propagated through all the trees by successive application of the relevant binary test to determine probability of belonging to a class c. When reaching a leaf node l_τ in all trees where $\tau \in [1, \ldots, T]$, posterior probabilities $P_\tau(c|V)$ are gathered in order to compute the final posterior probability of the pixel defined by $P(c|V) = \frac{1}{T}\sum_{\tau=1}^{T} P_\tau(c|V)$. Computation of class posterior probabilities in decision forest is illustrated in Fig. 2.

2.2   Statistical Shape and Appearance Model

The process of building the parametric statistical model of shape and appearance variations involves the task of building a shape model, an appearance model, and consecutively a combined model of shape and appearance priors. To build the shape model, a PDM [5] is built by equal angle sampling of the prostate contours to determine the landmarks automatically. The PDM of the contours are aligned to a common reference frame by generalized Procrustes analysis [13]. PCA of the aligned PDMs identifies the principal modes of shape variations. Posteriori probabilistic information (of pixels being prostate) of the segmented region are warped into correspondence using a piece-wise affine warp and are sampled from a shape-free reference similar to that of AAM [5]. PCA of the posterior probabilities from Section 2.1 is used to identify their principal modes of variation. The model may be formalized in the following manner. Let s and t represent the shape and posterior probability models, then

$$s = \overline{s} + \Phi_s\theta_s, \quad t = \overline{t} + \Phi_t\theta_t \tag{1}$$

where $\overline{s}$ and $\overline{t}$ denote the mean shape and posterior probability information respectively, then Φ_s and Φ_t contain the first p eigenvectors (obtained from 98% of total variations) of the estimated joint dispersion matrix of shape and posterior probability information and θ represent the corresponding eigenvalues. The model of shape and posterior probability variations are combined in a linear framework as,

$$b = \begin{bmatrix} W\theta_s \\ \theta_t \end{bmatrix} = \begin{bmatrix} W\Phi_s^T(s - \overline{s}) \\ \Phi_t^T(t - \overline{t}) \end{bmatrix} \tag{2}$$

where W denotes a weight factor (determined as in AAM [5]) coupling the shape and the probability space. A third PCA of the combined model ensures the reduction in redundancy of the combined model, and is given as,

$$b = E\alpha \tag{3}$$

where E is the matrix of eigenvectors and α the appearance parameters.

2.3   Optimization and Segmentation of a New Instance

In our model, we use the optimization framework similar to that proposed by Cootes et al. [5]. The objective function of our model is similar to AAM. However, instead of minimizing the sum-of-squared differences of intensities between the mean model and target image, we minimize the sum-of-squared differences of the posterior probabilities of the mean model and the target image. The prior knowledge of the optimization space is acquired by perturbing the combined model with known model parameters and perturbing the pose (translation, scale and rotation) parameters. Linear relationships between the perturbation of the combined model (δc) and the residual posterior probability values (δt) (obtained from the sum-of-squared differences between the posterior probabilities of the mean model and the target image), and between the perturbation of the pose parameters (δp) and the residual posterior probability values are acquired in multivariate regression frameworks as,

$$\delta c = R_c\delta t, \quad \delta p = R_p\delta t \tag{4}$$

R_c and R_p refer to the correlation coefficients. Given a test image, the posterior probability values of the pixels being prostate is determined with random forest soft classification. The sum-of-squared differences of the posterior probability values with the mean model is used to determine the residual value δt. The combined model (δc) and the pose parameters (δp) are then updated using Eq. (4) to generate a new shape, and combined model and consequently the new posterior probabilities. The process continues in an iterative manner until the difference of the mean model with the target image remains unchanged. The model is initialized at a resolution one fourth the size of the original image and the model propagates in a multi-resolution schema from lower to higher resolution to achieve segmentation.

Table 1. Prostate segmentation quantitative comparison (HD, MAD and MaxD in mm, Spec., Sens., and Acc., are for Specificity, Sensitivity and Accuracy respectively.) Statistically significant values are italicized

Method	DSC	HD	MAD	MaxD	Spec.	Sens.	Acc.
AAM [5]	0.94±0.03	4.92±0.96	2.15±0.94	5.3±0.48	0.89±0.03	0.993±0.006	0.97±0.009
Ghose et al. [11]	0.95±0.02	3.82±0.88	1.26±0.51	3.92±0.93	0.94±0.03	0.97±0.02	0.97±0.01
Our Method	*0.96±0.01*	*2.99±0.73*	*0.96±0.31*	3.01±0.73	0.94±0.02	0.991±0.005	0.98±0.007

3   Experimental Results and Discussions

We have validated the accuracy and robustness of our method with 24 axial mid-gland TRUS images of the prostate with a resolution of 354×304 pixels from 6 prostate datasets in a leave-one-patient-out evaluation strategy. The ground truth for the experiments are prepared in a schema similar to MICCAI prostate challenge 2009 [17], where manual segmentations performed by an expert radiologist were validated by an experienced urologist. Both doctors have over 15 years of experience in dealing with prostate anatomy, prostate segmentation, and ultrasound guided biopsies. We have fixed the number of trees to 100, tree depth to 30 and the lower bound of information gain to 10^{-7} in decision forest. These parameters were chosen empirically as they produced promising results with test images.

We have used most of the popular prostate segmentation evaluation metrics like DSC, 95% Hausdorff Distance (HD) [17], MAD [19], Maximum Distance (MaxD) [16], specificity [8], sensitivity, and accuracy [2] to evaluate our method. Furthermore, the results are compared with the traditional AAM [5], and to our previous work in which we used texture features extracted with quadrature filters in the statistical shape and appearance model [11]. It is observed from Table 1 that a probabilistic representation of the prostate regions in TRUS images significantly improves segmentation accuracy when compared to traditional AAM and to [11]. As opposed to the manual initialization of traditional AAM and as in [11], we use the posterior probability information for automatic initialization and training of our statistical shape and appearance model. We achieved a statistically significant improvement in t-test p-value for DSC, HD and MAD compared to traditional AAM [5] and to [11]. A high DSC value and low values of contour error metrics of HD and MAD are all equally important in determining the segmentation accuracy of an algorithm. In this context, we obtained better segmentation accuracies compared to [5] and [11]. To provide qualitative results of our method we present a subset of results in Fig. 3.

Our method is implemented in Matlab 7 on an Intel Core i5, 2.8 GHz processor and 8 GB RAM. The mean segmentation time of the method is 0.67±0.02 seconds with an unoptimized Matlab code. Even with an unoptimized Matlab

Table 2. Qualitative comparison of prostate segmentation

Reference	Area Accuracy	Contour Accuracy	Datasets	Time
Betrouni [3]	Overlap 93±0.9%	Distance 3.77±1.3 pixels	10 images	5 seconds
Shen [18]	Error 3.98±0.97%	Distance 3.2±0.87 pixels	8 images	64 seconds
Ladak [14]	Accuracy 90.1±3.2%	MAD 4.4±1.8 pixels	117 images	-
Cosio [6]	-	MAD 1.65±0.67 mm	22 images	11 minutes
Yan [19]	-	MAD 2.10±1.02 mm	19 datasets /301 images	0.3 seconds
Ghose [12]	DSC 0.96±0.01	MAD 0.80±0.24 mm	6 datasets/ 24 images	5.95 seconds
Our Method	DSC 0.96±0.01	MAD 3.44±1.11 pixels/ 0.96±0.31 mm	6 datasets/ 24 images	0.67 seconds

code in Table 2 we observe that our mean segmentation time is better when compared to [3], [18] and [6], although inferior to [19]. However, [19] used an optimized C++ code to achieve their results. We believe that a speed-up of computational time is possible with a parallelized and optimized code in GPU environment.

A quantitative comparison of different prostate segmentation methodologies is difficult in the absence of a public dataset and standardized evaluation metrics. Nevertheless, to have an overall qualitative estimate of the functioning of our method, we have compared with some of the existing 2D segmentation methods as shown Table 2. In Table 2, we may consider the area overlap and the area accuracy as equivalent of DSC measure and the average distance as equivalent of the average MAD. Analyzing the results, we observe that our mean DSC value is better than the area overlap accuracy values of Betrouni et al. [3] and Ladak et al. [14] and very similar to the area overlap error of Shen et al. [18]. However, it is to be noted that we have used more images compared to Shen et al. Our MAD value also shows improvement when compared to [3], [18], [14], [6] and [19]. From these observations we may infer our method performs well in overlap and contour accuracy measures when assessed qualitatively.

Furthermore, the obtained contour and area overlap accuracies are similar to the results obtained in [12]. In our previous work [12] we fused probabilities obtained from expectation maximization (EM) [7] based clustering and spatial probabilities to achieve a soft clustering of the prostate. In a schema similar to our proposed model in this article, automatic initialization and propagation of the deformable model was achieved with posterior probabilities. However, our previous work [12] was computationally more expensive due to the EM framework adopted for the model. Transforming the EM framework with a supervised learning framework, our proposed method achieves prostate segmentation in significantly less time than that required for [12]. The mean segmentation time of [12] with current machine configuration is 4.33±0.21 seconds while the proposed method using supervised learning with random forest takes 0.67±0.02 seconds without compromising the segmentation accuracies. Mean segmentation time is often a critical element in selecting one segmentation method over the other for
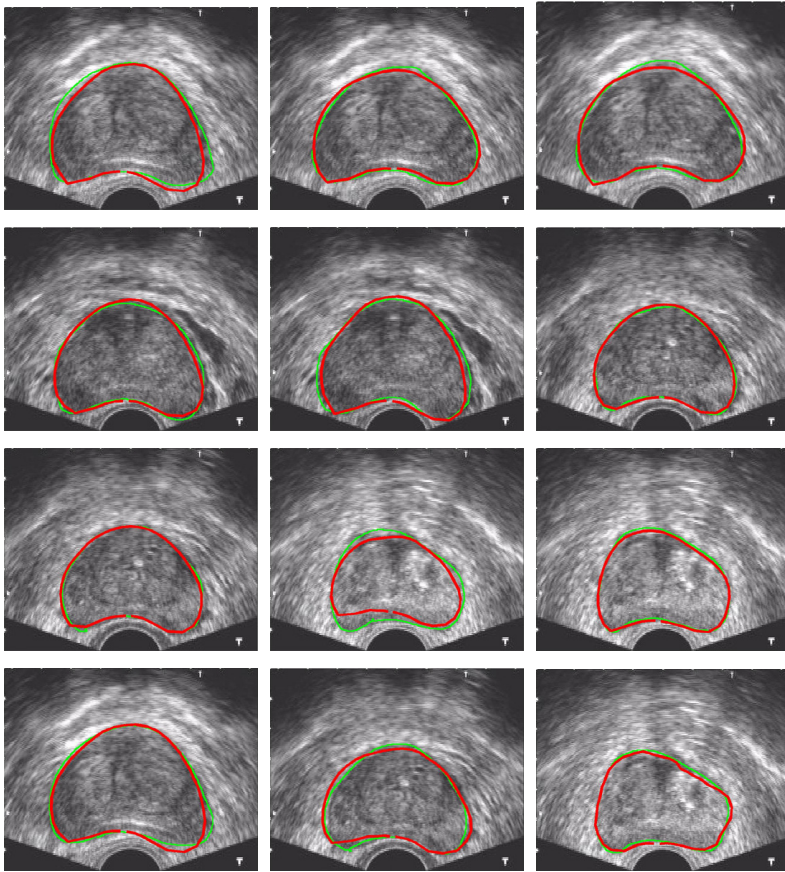
Fig. 3. The green contour gives the ground truth and the red contour gives the obtained result

near real-time multimodal image fusion between TRUS and MRI to improve malignant tissue sampling during biopsy. In this context, we may claim that our present method shows improvement over our previous work in [12].

4   Conclusion and Future Works

A novel approach of multiple statistical models of shape and posterior probability information of prostate region with the goal of segmenting the prostate in 2D TRUS images has been proposed. Our approach is accurate, and robust to significant shape, size and contrast variations in TRUS images compared to traditional AAM. While the proposed method is validated with prostate mid-gland images, effectiveness of the method for the base and the apical slices is yet to be validated.

References

1. Cancer Society Atlanta, A. Prostate Cancer (2011), `http://www.cancer.org` (accessed on January 28, 2012)
2. Badiei, S., Salcudean, S.E., Varah, J., Morris, W.J.: Prostate Segmentation in 2D Ultrasound Images Using Image Warping and Ellipse Fitting. In: Larsen, R., Nielsen, M., Sporring, J. (eds.) MICCAI 2006. LNCS, vol. 4191, pp. 17–24. Springer, Heidelberg (2006)
3. Betrouni, N., Vermandel, M., Pasquier, D., Maouche, S., Rousseau, J.: Segmentation of Abdominal Ultrasound Images of the Prostate Using A priori Information and an Adapted Noise Filter. Computerized Medical Imaging and Graphics 29, 43–51 (2005)
4. Cootes, T.F., Hill, A., Taylor, C.J., Haslam, J.: The Use of Active Shape Model for Locating Structures in Medical Images. Image and Vision Computing 12, 355–366 (1994)
5. Cootes, T.F., Edwards, G.J., Taylor, C.J.: Active Appearance Models. In: Burkhardt, H., Neumann, B. (eds.) ECCV 1998. LNCS, vol. 1407, pp. 484–498. Springer, Heidelberg (1998)
6. Cosío, F.A.: Automatic Initialization of an Active Shape Model of the Prostate. Medical Image Analysis 12, 469–483 (2008)
7. Dempster, A.P., Laird, N.M., Rubin, D.B.: Maximum Likelihood from Incomplete Data via the EM Algorithm. Journal of the Royal Statistical Society 39, 1–38 (1977)
8. Diaz, K., Castaneda, B.: Semi-automated Segmentation of the Prostate Gland Boundary in Ultrasound Images Using a Machine Learning Approach. In: Reinhardt, J.M., Pluim, J.P.W. (eds.) Procedings of SPIE Medical Imaging: Image Processing, pp. 1–8, SPIE, USA (2008)
9. Evangelidis, G.D., Emmanouil, Z.P.: Parametric Image Alignment Using Enhanced Correlation Coefficient Maximization. IEEE Trans. Pattern Anal. Mach. Intell. 30, 1858–1865 (2008)
10. Geremia, E., Menze, B.H., Clatz, O., Konukoglu, E., Criminisi, A., Ayache, N.: Spatial Decision Forests for MS Lesion Segmentation in Multi-Channel MR Images. In: Jiang, T., Navab, N., Pluim, J.P.W., Viergever, M.A. (eds.) MICCAI 2010. LNCS, vol. 6361, pp. 111–118. Springer, Heidelberg (2010)
11. Ghose, S., Oliver, A., Martí, R., Lladó, X., Freixenet, J., Mitra, J., Vilanova, J.C., Comet, J., Meriaudeau, F.: Statistical shape and texture model of quadrature phase information for prostate segmentation. International Journal of Computer Assisted Radiology and Surgery 7, 43–55 (2012)
12. Ghose, S., Oliver, A., Martí, R., Lladó, X., Freixenet, J., Vilanova, J.C., Meriaudeau, F.: A probabilistic framework for automatic prostate segmentation with a statistical model of shape and appearance. In: IEEE ICIP, pp. 713–716 (2011)
13. Gower, J.C.: Generalized Procrustes Analysis. Psychometrika 40, 33–51 (1975)
14. Ladak, H.M., Mao, F., Wang, Y., Downey, D.B., Steinman, D.A., Fenster, A.: Prostate Segmentation from 2D Ultrasound Images. In: Proceedings of the 22nd Annual International Conference of the IEEE Engineering in Medicine and Biology Society, pp. 3188–3191. IEEE Computer Society Press, Chcago (2000)

15. Li, W., Liao, S., Feng, Q., Chen, W., Shen, D.: Learning Image Context for Segmentation of Prostate in CT-Guided Radiotherapy. In: Fichtinger, G., Martel, A., Peters, T. (eds.) MICCAI 2011, Part III. LNCS, vol. 6893, pp. 570–578. Springer, Heidelberg (2011)
16. Liu, H., Cheng, G., Rubens, D., Strang, J.G., Liao, L., Brasacchio, R., Messing, E., Yu', Y.: Automatic Segmentation of Prostate Boundaries in Transrectal Ultrasound (TRUS) Imaging. In: Sonka, M., Fitzpatrick, J.M. (eds.) Proceedings of the SPIE Medical Imaging: Image Processings, pp. 412–423, SPIE, USA (2002)
17. MICCAI: 2009 prostate segmentation challenge MICCAI (2009), `http://wiki.na-mic.org/Wiki/index.php` (accessed on April 1, 2011)
18. Shen, D., Zhan, Y., Davatzikos, C.: Segmentation of Prostate Boundaries from Ultrasound Images Using Statistical Shape Model. IEEE Transactions on Medical Imaging 22, 539–551 (2003)
19. Yan, P., Xu, S., Turkbey, B., Kruecker, J.: Discrete Deformable Model Guided by Partial Active Shape Model for TRUS Image Segmentation. IEEE Transactions on Biomedical Engineering 57, 1158–1166 (2010)
20. Zhan, Y., Shen, D.: Deformable Segmentation of 3D Ultrasound Prostate Images Using Statistical Texture Matching Method. IEEE Transactions on Medical Imaging 25, 256–272 (2006)